

Seismoelectric effects due to mesoscopic heterogeneities

Damien Jougnot*

J. Germán Rubino*

Marina Rosas Carbajal

Niklas Linde

Klaus Holliger

Applied and Environmental Geophysics Group, University of Lausanne,
CH-1015 Lausanne, Switzerland.

* These authors contributed equally to this work

D. Jougnot, Applied and Environmental Geophysics Group, University of Lausanne, CH-1015
Lausanne, Switzerland. (Damien.Jougnot@unil.ch)

While the seismic effects of wave-induced fluid flow due to mesoscopic heterogeneities have been studied for several decades, the role played by these types of heterogeneities on seismoelectric phenomena is largely unexplored. To address this issue, we have developed a novel methodological framework which allows for the coupling of wave-induced fluid flow, as inferred through numerical oscillatory compressibility tests, with the pertinent seismoelectric conversion mechanisms. Simulating the corresponding response of a water-saturated sandstone sample containing mesoscopic fractures, we demonstrate for the first time that these kinds of heterogeneities can produce measurable seismoelectric signals under typical laboratory conditions. Given that this phenomenon is sensitive to key hydraulic and mechanical properties, we expect that the results of this pilot study will stimulate further exploration on this topic in several domains of the Earth, environmental, and engineering sciences.

1. Introduction

When a seismic wave propagates through a water-saturated porous medium, it produces a relative motion between the fluid phase and the rock matrix [*Biot*, 1956]. This flow transports an electrical excess charge, contained in the electrical double layer located along grain surfaces, thus producing an electrical current source. This is the physical principle of the seismoelectric phenomenon, which *Pride* [1994] formalized by coupling Biot's (1956) and Maxwell's equations.

For seismic waves propagating through water-saturated porous media, the theory predicts two kinds of seismoelectric conversions: (1) the coseismic field, and (2) the interface response. The coseismic field is a consequence of the wavelength-scale flow accompanying a compressional wave, which generates a current source even in homogeneous media. The resulting electric field travels with the wave and has a very limited extent outside of the support of the wave. Conversely, when a seismic wave encounters a contrast in mechanical or electrical properties, there is a corresponding variation in the current source distribution, thus generating electrical potential differences that can be measured outside of the wave support. The associated electric fields are highly sensitive to the fluid pressure gradients in the vicinity of the interface. Accurate modeling of seismic wave conversions at interfaces and, in particular, of the associated Biot slow waves, is therefore critical for a realistic simulation of the seismoelectric response [*Pride and Garambois*, 2002].

A particular interface-type response is expected to take place in the presence of mesoscopic heterogeneities, that is, heterogeneities having sizes larger than the characteristic pore scale but smaller than the prevailing wavelengths. It is well known that the propa-

gation of seismic waves through a medium containing these kinds of heterogeneities can induce significant oscillatory fluid flow as, in response to the spatial variations in elastic compliances, the stresses associated with the passing seismic wave produce a pore fluid pressure gradient. Indeed, the energy dissipation associated with this phenomenon is widely considered to be one of the most important intrinsic seismic attenuation mechanisms in the shallower parts of the crust [e.g., *Müller et al.*, 2010]. The characteristics of such wave-induced flow are mainly controlled by the compressibility contrast between the heterogeneities and the embedding matrix as well as permeabilities and geometrical characteristics of the heterogeneities. Given that the amount of flow produced by this phenomenon can be significant, corresponding strong seismoelectric signals carrying valuable information about these properties are also expected to arise.

Modeling wave-induced fluid flow is problematic because the corresponding diffusion lengths, that is, the spatial scales at which fluid flow occurs, are very small compared with the seismic wavelengths. Together with the theoretical complications arising from the coupling of the poro-elastic and electromagnetic responses, this may explain why the generation of seismoelectric effects due to mesoscopic heterogeneities is largely unexplored. Arguably, the most important work on this topic is by *Haartsen and Pride* [1997], who modeled the seismoelectric response from a single sand layer having a thickness much smaller than the predominant seismic wavelengths. More recently, *Zhu et al.* [2008] performed seismoelectric laboratory experiments demonstrating that electromagnetic waves are generated at horizontal fractures intersecting boreholes.

In this paper, we propose a novel approach to address this problem based on a numerical oscillatory compressibility test coupled with a model for seismoelectric conversion and signal generation. We illustrate the methodology by analyzing the electrical potential produced by mesoscopic fractures in an otherwise homogeneous water-saturated sandstone sample. The reason for this choice of model is that the amount of wave-induced fluid flow scales with the compressibility contrasts between the mesoscopic heterogeneities and their embedding matrix, which in turn implies that a particularly prominent seismoelectric response can be expected in fractured media.

2. Methodological background

We consider a square rock sample containing mesoscopic heterogeneities and apply a time-harmonic compression

$$P(t) = \Delta P \cos(\omega t), \quad (1)$$

at its top boundary, where ω is the angular frequency and t time. No tangential forces are applied on the boundaries of the sample and the solid is neither allowed to move on the bottom boundary nor to have horizontal displacements on the lateral boundaries. The fluid is not allowed to flow into or out of the sample. To obtain the response of the sample, we numerically solve the equations of quasi-static poroelasticity under corresponding boundary conditions [Rubino *et al.*, 2009]. This methodology allows for computing the relative fluid velocity field $\dot{\mathbf{w}}$ which is then employed to calculate the corresponding seismoelectric signal.

Wave-induced flow exerts a drag on the excess electrical charges of the double layer surrounding grain surfaces, thereby generating a source current density of the form [Jardani

et al., 2010]

$$\mathbf{j}_s = \bar{Q}_v^{eff} \dot{\boldsymbol{\omega}}, \quad (2)$$

where \bar{Q}_v^{eff} is the effective excess charge density.

In absence of an external current density, the electrical potential φ in response to a given source current density is described by [Sill, 1983]

$$\nabla \cdot (\sigma \nabla \varphi) = \nabla \cdot \mathbf{j}_s, \quad (3)$$

where σ denotes the electrical conductivity. Given the fluid velocity field $\dot{\boldsymbol{\omega}}$ inferred from the oscillatory compressibility test, the seismoelectric signal induced by the presence of mesoscopic heterogeneities is then obtained by numerically solving equations (2) and (3). As proposed by *Revil and Mahardika* [2013], we choose to ignore electroosmotic phenomena. Conversely, we assumed the electrical conductivity to be invariant with frequency because the frequency-dependence of the effects of the wave-induced fluid flow are orders-of-magnitudes larger than those of the electrical conductivity (see *Kruschwitz et al.* [2010] for electrical measurements on sandstones).

3. Numerical example: Seismoelectric response of fractured rocks

We consider a model of a homogeneous water-saturated clean sandstone permeated by three mesoscopic fractures (Figure 1a). The sample is a square with a side length of 2.5 cm, and the mean aperture of the fractures is $h = 0.033$ cm. The poroelastic response of this medium is modeled by representing the mesoscopic fractures as highly compliant and permeable porous regions embedded in a stiffer porous matrix [Rubino *et al.*, 2013]. The background and the fracture materials are hereafter denoted through the superscripts b and f [Rubino *et al.*, 2013]: drained-frame bulk moduli $K_m^b = 23$ GPa

and $K_m^f = 0.02$ GPa, shear moduli $\mu_m^b = 27$ GPa and $\mu_m^f = 0.01$ GPa, porosities $\phi^b = 0.1$ and $\phi^f = 0.5$, permeabilities $\kappa^b = 2.37 \times 10^{-14}$ m² and $\kappa^f = 10^{-10}$ m², and solid grain bulk moduli $K_s^b = K_s^f = 37$ GPa. The sample is fully saturated with water, with bulk modulus $K_w = 2.25$ GPa and viscosity $\eta_w = 0.003$ Pa s. The amplitude of the applied compression is $\Delta P = 1$ kPa.

We determine the electrical conductivities using $\sigma = \sigma_w \phi^m$, with m denoting the cementation exponent from Archie's law and σ_w the pore water conductivity. Given the considered medium, the surface conductivity can be neglected. We use $m^b=2$, $m^f=1.3$, and $\sigma_w = 10^{-2}$ S/m, which represents a typical value for pore water conductivity in laboratory experiments.

The simulated flow is in the viscous laminar regime and we can therefore estimate the effective excess charge for the two materials using the empirical relationship proposed by *Jardani et al.* [2007]

$$\log(\bar{Q}_v^{eff}) = -9.2349 - 0.8219 \log(\kappa). \quad (4)$$

This yields $\bar{Q}_v^{eff,b}=87.6$ C/m³ and $\bar{Q}_v^{eff,f}=9.33 \times 10^{-2}$ C/m³. These values are consistent with those obtained by *Jouniaux and Pozzi* [1995] from voltage coupling coefficient measurements on sandstones with similar permeabilities.

Figure 1 displays the horizontal (x) and vertical (y) components of the relative fluid velocity field at $t = 0$ in equation (1). For 1 Hz (Figures 1b and 1d), we observe that the induced fluid velocity field is negligible. This is expected, as for such a low frequency the diffusion lengths are larger than the size of the considered heterogeneities and there is enough time during each oscillatory half-cycle for the pore fluid pressure to equilibrate

to a common value. For a frequency of 10 kHz, the oscillatory compression produces a significant fluid pressure increase in the highly compliant fractures as compared to the stiffer embedding matrix, thus establishing an important fluid pressure gradient. Correspondingly, the amount of fluid flow is much more important in this case (Figures 1c and 1e). Significant fluid flow occurs inside the fractures (Figure 1c), but there is also an important fluid exchange between the fractures and the embedding matrix material (Figure 1e).

The relative fluid velocity field obtained from the oscillatory compressibility test is used to solve the electrical problem through equations (2) and (3). Neumann boundary conditions (electrical insulation) are considered at the boundaries of the sample, in conjunction with a Dirichlet boundary condition ($\varphi = 0$ V) at the right bottom corner of the sample ($x = 2.5$ and $y = 0$ cm).

Figures 2a and 2b show the electrical potential at $t = 0$ for 1 Hz and 10 kHz, respectively. The magnitude and distribution of the seismoelectric signal strongly depends on the frequency of the applied compression. In particular, the fluid flow occurring in the vicinity of the fractures induces at 10 kHz an important divergence of the source current density \mathbf{j}_s , which in turn generates seismoelectric signals with measurable amplitudes of a few mV (Figure 2b). For a frequency of 1 Hz, the signal is too small to be measured (Figure 2a), which is expected given the smaller magnitude of fluid flow (Figures 1b and 1d).

To evaluate the feasibility of observing such seismoelectric signals in laboratory experiments, we consider the responses at two measurement electrodes with respect to a

reference electrode ($\varphi = 0$ V) as functions of “normalized” time ($t \times f$) (Figures 2c and 2d). While no clear signal can be seen for a frequency of 1 Hz (Figure 2c), the seismoelectric responses are on the order of a few mV at 10 kHz (Figure 2d), which can be readily measured under laboratory conditions. We also observe a discrepancy, both in magnitude $|\varphi|$ and phase θ , between the two electrodes simulated for this higher frequency. Indeed, even though the electrode located at the top boundary is further from the reference than the one located in the middle, its signal is 1.8 times weaker. This electrode is almost in phase ($\theta \approx 20^\circ$) with the oscillatory compression, while the middle electrode shows a more important phase shift ($\theta \approx 140^\circ$). This phase shift is due to both the viscosity-related lag experienced by the wave-induced fluid flow and the relative position of the electrode with respect to the fractures.

Additional tests were conducted for a wide frequency range using different background permeabilities. Figures 3a and 3b show that the electrical potential measured at the top electrode is strongly frequency-dependent in terms of its amplitude and phase. The amplitude has a first peak at a frequency that depends on the background permeability, followed by a general increase at higher frequencies (Figure 3a). The phase spectrum also shows a dependence on κ^b , as the transition from high to low phase angles θ shifts to lower frequencies as the background permeability decreases (Figure 3b). These spectral signatures are explained by the fact that the frequency range where fluid flow prevails scales with the background permeability, together with the effects produced by the variations of the effective excess charge according to equation (4).

4. Discussion

When a seismic wave is incident perpendicular to a mesoscopic fracture plane, or equivalently, when an oscillatory compression is applied to a rock sample containing sub-horizontal fractures, an oscillatory flow is induced from the fracture into the pore space of the embedding matrix and vice versa. The spatial scales at which this flow occurs is limited by the spacing between the fractures and characterized by the diffusion length $L_d \equiv \sqrt{D/\omega}$, where D is the pressure diffusivity of the embedding matrix, a parameter directly proportional to the background permeability. Therefore, the frequency range where significant flow prevails scales with this hydraulic parameter and the spacing between the fractures. The amount of fluid flow is mainly governed by the compressibility contrast between the fractures and the embedding matrix. Therefore, while the frequency dependence of the seismoelectric signal is mainly governed by the separation between fractures and the embedding matrix permeability, its magnitude is expected to be controlled by the compressibility contrast between the fractures and the background, in addition to the permeability of the background, which also affects the effective excess charge (equation 4).

Additional numerical simulations indicate that the seismoelectric signal is highly sensitive to the orientation of the fractures. This is expected, as the amount of fluid flow in response to a vertical compression is maximum for sub-horizontal fractures and minimum for the sub-vertical case [Rubino *et al.*, 2013]. Moreover, fracture connectivity is also expected to play an important role in determining the characteristics of seismoelectric signals [Rubino *et al.*, 2013]. Consequently, the seismoelectric responses due to mesoscopic

effects are expected to contain key information on structural and hydraulic properties of the rock samples.

The most relevant result of this work is that mesoscopic heterogeneities can produce measurable seismoelectric signals in response to an oscillatory compression (Figures 2 and 3). Corresponding laboratory experiments are already conducted for seismic purposes [e.g. *Batzle et al.*, 2006], and could be extended to seismoelectric measurements. Although our analysis was performed considering laboratory-size samples, the results of this study also have corresponding implications for seismoelectric conversions at the field scale. Due to ubiquitous fractal scaling laws, virtually all geological formations contain mesoscopic heterogeneities and, therefore, seismic waves will produce seismoelectric signals as they travel through such heterogeneities. Indeed, it is likely that some of the notorious difficulties encountered in seismoelectric field applications, notably the generally high noise levels [e.g. *Strahser et al.*, 2011], could be related to heterogeneities of different nature and sizes, yielding a multiplicity of seismoelectric source currents dispersed over the volume traversed by the seismic waves. A better understanding of the role played by mesoscopic heterogeneities is therefore needed to improve the generation, recording and interpretation of seismoelectric signals.

5. Conclusions

Based on a novel methodological framework that couples recent improvements in the modeling of wave-induced fluid flow and seismoelectric conversion mechanisms, we have shown for the first time that the presence of mesoscopic heterogeneities can produce measurable seismoelectric signals for typical laboratory setups. In particular, we find a

measurable frequency-dependent response of the seismoelectric signal caused by mesoscopic fractures in an otherwise homogeneous water-saturated sandstone sample. The magnitude of the seismoelectric signal is mainly governed by the compressibility contrast between the embedding matrix and the mesoscopic heterogeneities. Therefore, prominent seismoelectric effects are expected to arise not only in fractured media, but also in partially saturated porous rocks. This in turn opens the perspective of developing seismoelectric spectroscopy as a novel method for characterizing such media.

Given the ever increasing interest in the measurement and interpretation of seismoelectric signals, the results of this pilot study are expected to be of interest in a wide range of domains of the Earth, environmental, and engineering sciences, including nondestructive testing, groundwater and contaminant hydrology, hydrothermal operations, nuclear waste storage as well as hydrocarbon exploration and production, among many others. Correspondingly, further computational and experimental work on this topic is needed, as it promises to provide deeper insights on the dependence of the recorded signals on pertinent hydraulic and mechanical properties as well as to improve the acquisition, recording, and interpretation of seismoelectric data *per se*.

Acknowledgments. This work was supported in part by grants from the Swiss National Science Foundation. The authors modified Mafplot (maflot.com), kindly provided by I. Lunati and R. Kunze. The authors thank the Editor Michael Wysession and two anonymous reviewers for constructive comments that helped to improve the quality of this manuscript.

References

- Batzle, M., D. Han, and R. Hofmann, Fluid mobility and frequency-dependent seismic velocity - Direct measurements, *Geophysics*, *71*(1), N1–N9, 2006.
- Biot, M., Theory of propagation of elastic waves in a fluid saturated porous solid. I. Low frequency range, *J. Acoust. Soc. Amer.*, *28*, 168–178, 1956.
- Haartsen, M., and S. Pride, Electro seismic waves from point sources in layered media, *J. Geophys. Res.*, *102*(B11), 24,745–24,769, 1997.
- Jardani, A., A. Revil, A. Bolève, A. Crespy, J. Dupont, W. Barrash, and B. Malama, Tomography of the Darcy velocity from self-potential measurements, *Geophys. Res. Lett.*, *34*(24), L24,403, 2007.
- Jardani, A., A. Revil, E. Slob, and W. Söllner, Stochastic joint inversion of 2D seismic and seismoelectric signals in linear poroelastic materials: A numerical investigation, *Geophysics*, *75*, N19–N31, 2010.
- Jouniaux, L., and J. Pozzi, Permeability dependence of streaming potential in rocks for various fluid conductivities, *Geophys. Res. Lett.*, *22*(4), 485–488, 1995.
- Kruschwitz, S., A. Binley, D. Lesmes, and A. Elshenawy, Textural controls on low-frequency electrical spectra of porous media, *Geophysics*, *75*(4), WA113–WA123, 2010.
- Müller, T., B. Gurevich, and M. Lebedev, Seismic wave attenuation and dispersion resulting from wave-induced flow in porous rocks - A review, *Geophysics*, *75*, A147–A164, 2010.
- Pride, S., Governing equations for the coupled electromagnetics and acoustics of porous media, *Phys. Rev. B*, *50*, 15,678–15,696, 1994.

- Pride, S., and S. Garambois, The role of Biot slow waves in electroseismic wave phenomena, *J. Acoust. Soc. Am.*, *111*(2), 697–706, 2002.
- Revil, A., and H. Mahardika, Coupled hydromechanical and electromagnetic disturbances in unsaturated porous materials, *Water Resour. Res.*, *49*, 1–23, 2013.
- Rubino, J., C. Ravazzoli, and J. Santos, Equivalent viscoelastic solids for heterogeneous fluid-saturated porous rocks, *Geophysics*, *74*, N1–N13, 2009.
- Rubino, J. G., L. Guarracino, T. M. Müller, and K. Holliger, Do seismic waves sense fracture connectivity?, *Geophys. Res. Lett.*, doi:10.1002/grl.50127, 2013.
- Sill, W., Self-potential modeling from primary flows, *Geophysics*, *48*(1), 76–86, 1983.
- Strahser, M., L. Jouniaux, P. Sailhac, P.-D. Matthey, and M. Zillmer, Dependence of seismoelectric amplitudes on water content, *Geophys. J. Int.*, *187*(3), 1378–1392, 2011.
- Zhu, Z., M. N. Toksöz, and D. R. Burns, Electrostatic and seismoelectric measurements of rock samples in a water tank, *Geophysics*, *73*(5), E153–E164, 2008.

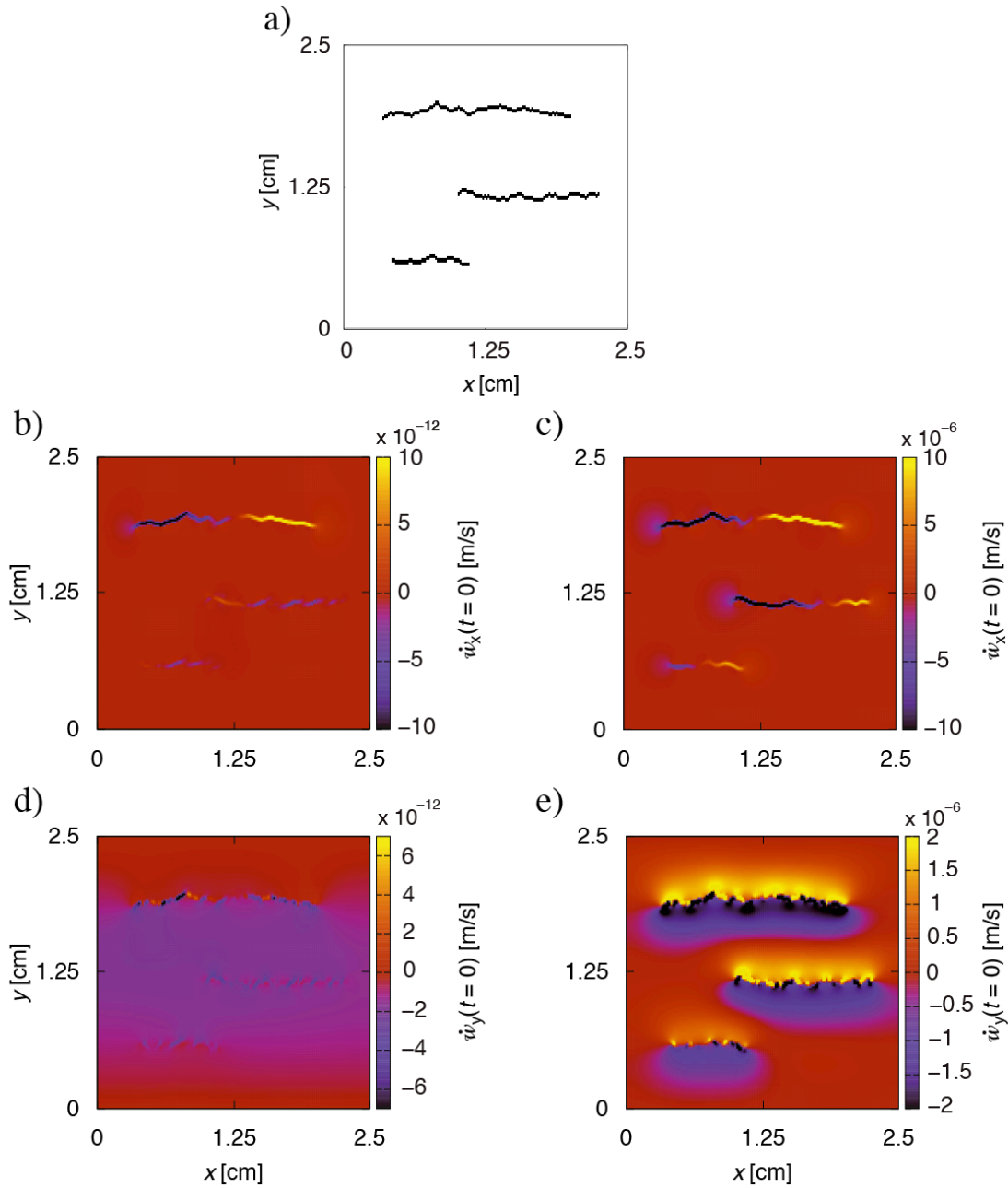


Figure 1. (a) Numerical sample with three fractures. (b and c) Horizontal and (d and e) vertical components of the relative fluid velocity field at $t = 0$ in equation (1). The results correspond to an oscillatory compressibility test with an amplitude of 1 kPa and frequencies of (b and d) 1 Hz and (c and e) 10 kHz.

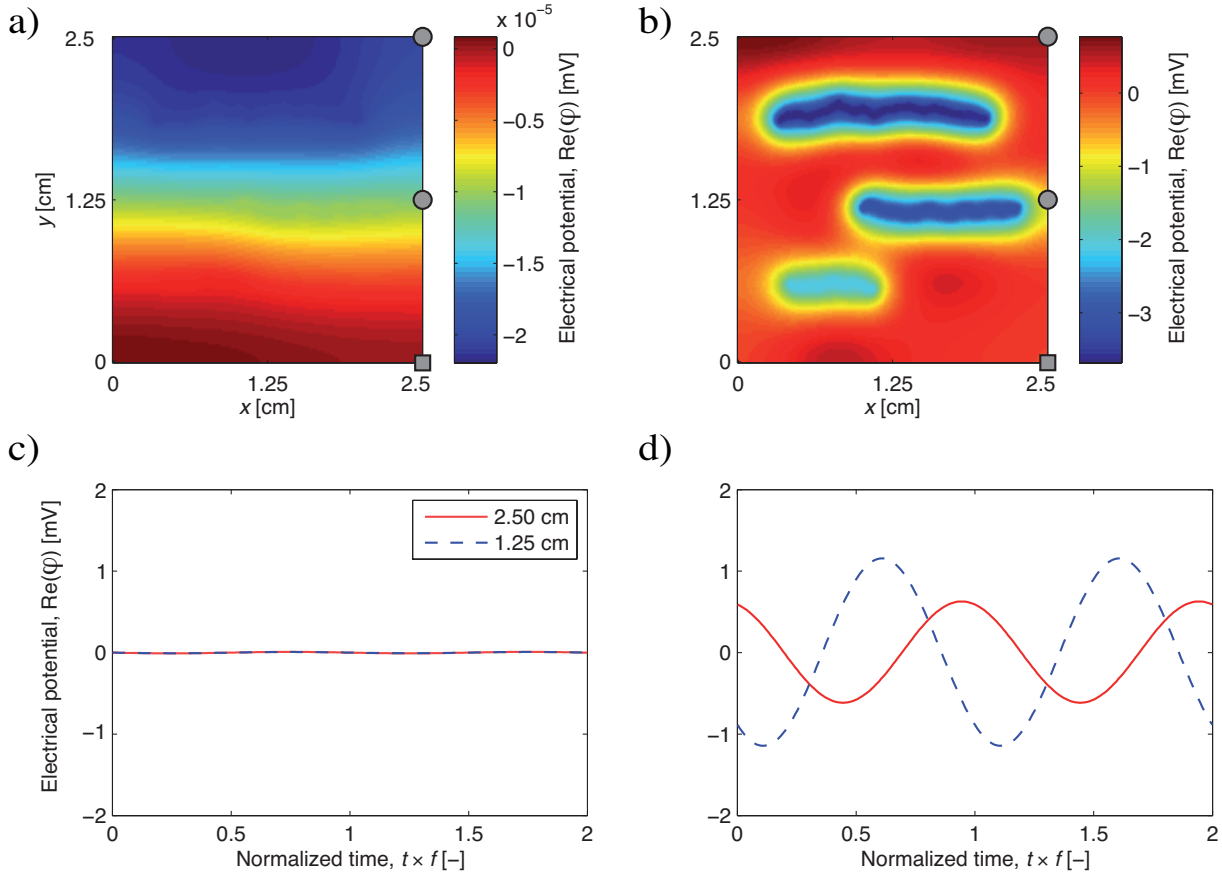


Figure 2. (a and b) Electrical potential distribution at $t = 0$ in equation (1) and (c and d) resulting electrical potential differences at two electrodes with respect to the reference electrode as functions of the normalized time. The grey square and the two circles (in a and b) highlight the position of the reference and the potential electrodes, respectively. The results correspond to an oscillatory compressibility test with an amplitude of 1 kPa and frequencies of (a and c) 1 Hz and (b and d) 10 kHz.

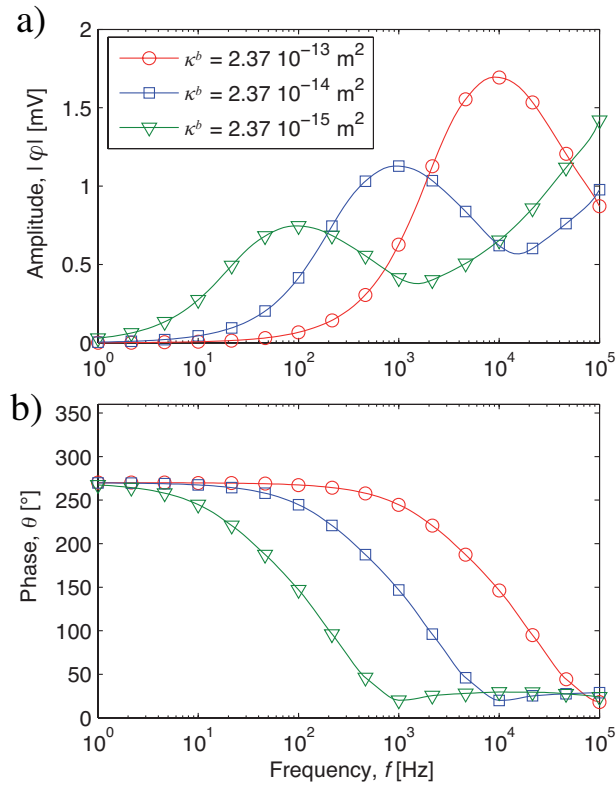


Figure 3. Effect of background permeability upon (a) the amplitude $|\varphi|$ and (b) the phase θ of the electrical voltage recorded at the top electrode ($y = 2.5$ cm) for different frequencies.